Acta Cryst. (1982). B**38**, 2121–2133

Structure of Magnetite (Fe_3O_4) below the Verwey Transition Temperature*

BY M. IIZUMI†

Japan Atomic Energy Research Institute, Tokai 319-11, *Japan*

T. F. KOETZLE AND G. SHIRANE

Brookhaven National Laboratory, Upton, New York 11973, *USA*

AND S. CHIKAZUMI, M. MATSUI‡ AND S. TODO

Institute for Solid State Physics, University of Tokyo, Roppongi, Minato-ku, Tokyo 106, *Japan*

(*Received* 1 *September* 1981; *accepted* 24 *February* 1982)

Abstract

The structure of Fe_3O_4 at 10 K, a temperature below that of the Verwey transition ($T_V \simeq 120$ K), has been analyzed with three-dimensional neutron diffraction data. The space group is found to be *Cc* with a monoclinic unit cell which corresponds to $\sqrt{2}a \times \sqrt{2}a \times 2a$ of the cubic spinel unit cell (space group *Fd*3*m*) found above T_V. The monoclinic cell contains 32 formula units. In order to facilitate analysis of this complicated structure, primitive orthorhombic space groups with pseudosymmetric elements have been adopted as approximations. The displacements of atoms from the cubic positions have been decomposed into distinct displacement patterns with characteristic symmetries, which suggest that the displacements brought about by the phase transition result from the simultaneous condensation of a few phonons.

Introduction

The phase transition in magnetite at about 120 K was postulated by Verwey and co-workers (Verwey, Haayman & Romeijan, 1947) to be an electronic phase transition in which charge ordering takes place among Fe ions on the octahedral or *B* sites. In the ordering scheme proposed by Verwey *et al.* [110] and [1$\bar{1}$0] rows of *B* sites on the (001) planes of the spinel structure are occupied alternately by Fe^{2+} and Fe^{3+}. This ordering scheme was apparently verified by the observation of the 002 magnetic reflection with neutrons (Hamilton, 1958).

Recently, however, a number of experimental observations have made it necessary to abandon this simple model. Firstly, the orthorhombic symmetry underlying the Verwey model has been disproved by electron diffraction (Chikazumi, Chiba, Suzuki & Yamada, 1971) and by X-ray (Iida, Yamamoto & Umemura, 1973; Vieland, 1975) and neutron (Shirane, Chikazumi, Akimitsu, Chiba, Matsui & Fujii, 1975; Iizumi & Shirane, 1975) diffraction. These experiments have clearly established the rhombohedral distortion of the cubic unit cell, which was first detected from X-ray powder diffraction photographs (Toombs & Rooksby, 1951). Secondly, the detailed neutron diffraction measurements (Shirane *et al.*, 1975) proved that the intensity of 002-type reflections is actually zero when the contribution from simultaneous reflections is carefully removed.

A more complicated situation has been suggested by the discovery of superlattice reflections below T_V with neutron (Samuelson, Bleeker, Dobrzynski & Riste, 1967, 1968) and electron (Yamada, Suzuki & Chikazumi, 1968) diffraction. These superlattice reflections have their principal origin in atomic displacements developing below T_V. The phase transition is quite complex and, in order to be plausible, a model should relate the charge ordering to the atomic displacements in a realistic manner.

In order to elucidate this situation Fujii, Shirane & Yamada (1974) studied the critical scattering of neutrons which appears just above T_V at the same points where the superlattice reflections evolve. They showed that the Verwey transition is related to a lattice instability characterized by Δ_5 symmetry with wave-vector $\mathbf{q}_\Delta = (0,0,\frac{1}{2})$ and pointed out that the charge-density fluctuations which can couple with the lattice instability are quite different from the charge-ordering scheme proposed by Verwey. A theoretical counterpart to this study was set forth by Yamada (1975) in

* Research carried out under contract with the US Department of Energy and supported by its Office of Basic Energy Sciences.

† Guest scientist at Brookhaven National Laboratory, now returned.

‡ Now at the Faculty of Engineering, Nagoya University, Furocho, Chigusa-ku, Nagoya 464, Japan.

0567-7408/82/082121-13$01.00

which he proposed a general idea of the dynamical instability of the coupled mode between the charge-density wave and phonon. He also proposed a specific model in which the Δ_5 phonons at $\mathbf{q}_\Delta$ play an essential role. Hereinafter we call the latter part of this theory the Yamada model.

Yamada concerned himself solely with the atomic displacements characterized by the wavevector $\mathbf{q}_\Delta$ which give rise to the half-integer-type superlattice reflections $(h, k, l + \frac{1}{2})$. A set of atomic displacements given by Yamada explains these half-integer reflections quite well, provided use is made of the experimental observation that only one of the doubly degenerate Δ_5 modes condenses at the transition (Iizumi & Shirane, 1975). However, there are additional superlattice reflections of the even–odd mixed-integer type (for example, $h + l = 2n + 1$) and the explanation of their intensities is beyond the scope of the Yamada model (Shirane *et al.*, 1975; Iizumi & Shirane, 1975).

Experimental verification of the charge ordering is a complicated problem. The change in intensity of the magnetic reflection of neutrons through the transition consists of two components:

$$\Delta F_M(Q) = \sum \Delta P_j e^{i\mathbf{Q}\cdot\mathbf{r}_j} + i \sum \bar{P}(\mathbf{Q}.\Delta_j) e^{i\mathbf{Q}\cdot\mathbf{r}_j}. \quad (1)$$

The first term represents the change of the magnetic scattering with the charge modulation. ΔP_j indicates an increment of magnetic moment of an Fe ion at $\mathbf{r}_j$. The second term is induced by displacement of the magnetic ions. $\bar{P}$ is an average magnetic moment of B-site Fe ions [4·5 μ_B (1 Bohr magneton $\equiv 9{\cdot}3 \times 10^{-24}$ J T^{-1})] and Δ_j is a displacement of an ion from the equilibrium position in the cubic phase. The latter term is not negligible; for many reflections it constitutes a principal part. Thus the charge-ordering scheme cannot be decided until the crystal structure in the low-temperature phase is known. This situation prompted us to attempt the present work. Here we describe the crystal structure determined from the three-dimensional neutron diffraction data. The determination of the charge ordering based on the present crystal structure requires further measurements.

In the cubic prototype inverse spinel structure above T_V, there are eight formula units in a unit cell ($a_0 =$ 8·3940 Å). The atoms occupy special positions in the space group $Fd3m$ as follows: positions 8(a) which are usually designated A sites are occupied by Fe^{3+} ions, positions 16(d) designated B sites are randomly occupied by equal numbers of Fe^{2+} and Fe^{3+} ions, while the positions 32(e) of the O^{2-} ions deviate slightly from the ideal structure in which $u = \frac{1}{4}$ and O atoms form face-centered cubic sublattices.* The parameter u in Fe_3O_4 has been determined by Hamilton (1958) to be 0·2548 (2)* at 296 K.

It is convenient to use the cubic indexing of reflections even below T_V. Below T_V the c axis is uniquely defined because of field cooling and two types of superlattice reflections appear: half-integer $(h, k, l + \frac{1}{2})$ and even–odd mixed integer ($h + k = 2n + 1$; $h + l = 2n + 1$; $k + l = 2n + 1$). The former arise from doubling of the unit cell along the **c** direction, while the latter result from loss of the f.c.c. translation. It is helpful to adopt a more detailed classification, in which wavevector terminology is employed to characterize the superlattice reflections. Reciprocal-lattice vectors **H** are comprised of

$$\mathbf{H} = \mathbf{H}_0 + \mathbf{q}, \quad (2)$$

where $\mathbf{H}_0$ belongs to the original f.c.c. lattice above T_V and $\mathbf{q}$ is a wavevector within the first Brillouin zone. These vectors are represented by three components, *e.g.* $\mathbf{H}_0 = (h,k,l)$ where h, k, and l are either all-odd or all-even integers. The fundamental reflections are characterized by $\mathbf{q} = 0$, while the superlattice reflections have one of the following $\mathbf{q}$ vectors and are designated by the conventional notation for symmetry points in the Brillouin zone.

$$\begin{array}{lll} \Delta & \Delta \text{ type} & \mathbf{q}_\Delta = (0,0,\frac{1}{2}) \\ W & \begin{cases} W_x \text{ type} & \mathbf{q}_{W(x)} = (1,0,\frac{1}{2}) \\ W_y \text{ type} & \mathbf{q}_{W(y)} = (0,1,\frac{1}{2}) \end{cases} \\ Z & X_z \text{ type} & \mathbf{q}_{X(z)} = (0,0,1) \\ X & \begin{cases} X_x \text{ type} & \mathbf{q}_{X(x)} = (1,0,0) \\ X_y \text{ type} & \mathbf{q}_{X(y)} = (0,1,0) \end{cases} \end{array} \quad (3)$$

The former three types constitute the half-integer reflections and the latter three the mixed-integer reflections.

Neutron diffraction measurements do not show any significant differences between W_x and W_y or between X_x and X_y. Therefore, the W_x and W_y reflections may be grouped together as the W type and the X_x- and X_y-type reflections grouped as the X type. In contrast, the X_z type shows distinct differences from the X_x and X_y type and is termed the Z type.†

Two special classes of the fundamental reflections deserve attention. Reflections $0kl$: $k + l = 4n + 2$ and their cyclic interchanges are missing above T_V because of the diamond glide in the spinel structure and are very weak below T_V. Reflections hkl: $h, k = 4n, l = 4n + 2$ are very weak because of the small deviation of the u parameter from $\frac{1}{4}$. We call these reflection types D and U, respectively.

* The origin of the cubic unit cell is taken at the inversion center ($\bar{3}m$), and the coordinates of the O positions are designated u,u,u *etc.*

* Estimated standard deviations are given in parentheses in units of the last digit, here and throughout this paper.

† The notation Z should not be confused with the symbol Z used for designating a different symmetry line in the Brillouin zone.

The rhombohedral distortion of the cubic unit cell, the doubling of the cell along **c** (magnetically the easiest axis, *i.e.* the direction of magnetization), and the existence of a **c** glide indicate that the crystal has monoclinic symmetry with axial system [110], [1$\bar{1}$0] and [001] of the original cubic lattice. The **c** glide is derived from the absence of h, h, $l + \frac{1}{2}$ type reflections (Iizumi & Shirane, 1975). The occurrence of the X- and W-type superlattice reflections indicates that the extinction rule, $h + k = 2n$, related to the f.c.c. translation in the basal plane is lost in the low-temperature phase. This requires that $\sqrt{2}a$ be taken as translations along the [110] and [1$\bar{1}$0] axes. The unit cell is defined by

$$\begin{aligned} \mathbf{a}_M &= -\mathbf{a}_R - \mathbf{b}_R \\ \mathbf{b}_M &= \mathbf{a}_R - \mathbf{b}_R \\ \mathbf{c}_M &= 2\mathbf{c}_R, \end{aligned} \tag{4}$$

where $\mathbf{a}_R$, $\mathbf{b}_R$ and $\mathbf{c}_R$ are the sides of the rhombohedrally distorted cell (Fig. 1). the sense of $\mathbf{a}_M$ and $\mathbf{b}_M$ has been chosen in order to make the β angle obtuse. The reflection indices in the monoclinic system h_M, k_M and l_M are related to the cubic indices h, k, and l by

$$\begin{aligned} h_M &= -h - k \\ k_M &= h - k \\ l_M &= 2l. \end{aligned} \tag{5}$$

Since half-integer reflections are not observed with respect to h and k, h_M and k_M satisfy

$$h_M + k_M = 2n, \tag{6}$$

which means that the monoclinic lattice is C-centered and the space group is then Cc. If the weak X- and W-type reflections are assumed to be completely absent, space group Pc is obtained with a unit cell defined by $\mathbf{a}_M/2$, $\mathbf{b}_M/2$ and $\mathbf{c}_M$. This space group was confirmed by X-ray measurements (Yoshida & Iida, 1976).

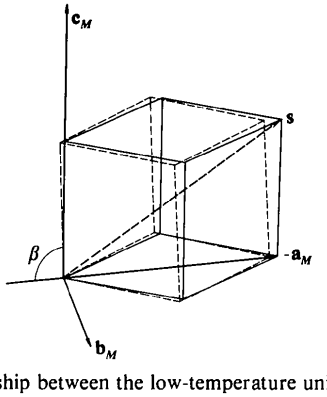

Fig. 1. Relationship between the low-temperature unit cell ($\mathbf{a}_M$, $\mathbf{b}_M$, $\mathbf{c}_M$) and the rhombohedrally distorted cell (solid lines). The cubic unit cell is dashed; the detwinning procedure involved squeezing around cubic [111], **S**.

Rado & Ferrari (1975, 1977) and Siratori *et al.* (1979) have observed the magnetoelectric effect which implies that the true space group is $P1$. The confirmation of such a triclinic structure is beyond the accuracy of current diffraction techniques. The displacements that violate the **c**-glide symmetry, if any, are extremely small compared with the main displacements which are compatible with the **c** glide.

Experimental

Crystal data and other experimental details are summarized in Table 1. Measurements were carried out on a single-domain crystal of synthetic Fe_3O_4, which was ground into the form of a cylinder approximately 3 mm in diameter and 6 mm in length with its axis parallel to cubic [111]. The sample was mounted in a closed-cycle helium refrigerator (Air Products and Chemicals, Inc. DISPLEX® model CS-202). Detwinning of the sample was accomplished by simultaneous application of field cooling and squeezing (Chikazumi, 1976). The sample was closely surrounded by a few aluminum rings and squeezed around [111] by the thermal contraction of the rings at low temperature. A magnetic field of about 1 T was applied along [001] in order to establish the c axis along that direction. The field was removed after cooling through T_V.

The sample was placed on an automated four-circle diffractometer (Dimmler, Greenlaw, Kelley, Potter, Rankowitz & Stubblefield, 1976; McMullan, Andrews, Koetzle, Reidinger, Thomas & Williams, 1976) at the Brookhaven High Flux Beam Reactor. A Be (110) single-crystal monochromator was employed to obtain a neutron beam of wavelength $\lambda = 0{\cdot}8387$ Å (based on Al_2O_3, hexagonal, $a = 4{\cdot}758$, $c = 12{\cdot}991$ Å at 298 K). An Er filter was used in order to suppress the contribution of $\lambda/2$ neutrons.

If the field-cooling and squeezing procedures are not completely effective, the Fe_3O_4 crystal may become

Table 1. *Crystal data and experimental details for magnetite* (Fe_3O_4, $T = 10$ K)

a_M	11·868 (2) Å
b_M	11·851 (2)
c_M	16·752 (4)
β	90·20 (3)°
V	2356·2 (8) Å^3
D_c ($Z = 32$)	5·221 Mg m^{-3}
μ*	0·0057 mm^{-1}
Maximum and minimum transmission factors	0·986, 0·981
(sin θ/λ) (max.)	0·64 Å^{-1}
Number of reflections measured	2160
Number of unique (orthorhombic) reflections	1465
$R_c = \sum_{hkl} \sum_{i=1}^{n} \lvert\langle F_o^2\rangle - F_{o,i}^2\rvert / \sum_{hkl} n \langle F_o^2\rangle$	0·046

* Mass absorption coefficients for Fe and O were obtained from *International Tables for X-ray Crystallography* (1968).

twinned. Three possibilities were investigated: (1) twins in which the c_M axis is not established along the direction of the magnetic field, (2) $[a,b]$ twins in which the a_M and b_M axes are intermixed, and (3) $[a,-a]$ twins in which the direction of the a_M axis is mutually reversed. The first type was checked by comparing the missing $\frac{1}{2}04$ and $0\frac{1}{2}4$ reflections with $40\frac{1}{2}$. The intensities of the former were less than 0·02 times that of the latter. The second type of twin was investigated by comparing the intensity of $44\frac{1}{2}$ with that of $\bar{4}4\frac{1}{2}$. The ratio $I(44\frac{1}{2})/I(\bar{4}4\frac{1}{2})$ was observed to be approximately 0·01. The $[a,-a]$ twin would reveal itself in splitting of the $hh0$ reflections. Although the strong reflections such as 440 did show splitting, the intensity ratio of the split peaks did not give a reliable estimate of the twin ratio because of the extinction. The intensity ratio 0·03 of the split $40\frac{1}{2}$ peaks therefore was taken as a measure of the population of the $[a,-a]$ twins, although this is only strictly appropriate for orthorhombic symmetry, as discussed below.

The sample was maintained at a temperature of 10 ± 0·5 K during the experiment, as measured by means of a Ge resistance thermometer placed in close proximity to the crystal. Monoclinic unit-cell constants listed in Table 1 were obtained by a least-squares procedure, based on observed sin θ values for 19 reflections.

Intensities were measured for a total of 2160 reflections out to a 2θ limit of 65°. Of these, 1551 reflections lie in octant $h_M k_M l_M$ and the remaining 604 reflections in octant $h_M k_M \bar{l}_M$. To check experimental stability, the 0,0,16 and 081 reflections were monitored every 30 measurements. These monitor reflections showed no significant variation in intensity beyond that expected from counting statistics. A θ:2θ step-scan procedure was adopted, with the scan range $\Delta 2\theta$ = 1·92° and 48 steps per scan. At each step, counts were accumulated for approximately 4 s, with the exact time interval determined by continuously monitoring the incident neutron flux. Integrated intensities were obtained, with the last three steps on either end of each scan taken as a measure of the background, and corrected for absorption by the Gaussian numerical-integration method (Busing & Levy, 1957). The cylindrical crystal shape was approximated by 14 boundary planes with rational indices. Finally, values of F_o^2 were obtained as $I \sin 2\theta$.

The intensities measured in the second octant were generally observed to agree quite well with corresponding measurements in the first octant. Therefore, values of F_o^2 were averaged for $h_M k_M l_M$ and $h_M k_M \bar{l}_M$, to calculate the mean $\langle F_o^2 \rangle$ and associated standard deviation based on counting statistics $\sigma_c(\langle F_o^2 \rangle)$. The overall agreement factor is 0·046, as indicated in Table 1. Of 479 reflections scanned in both octants, only nine had individual intensities that differed by more than five e.s.d.'s from the mean. (For purposes of this comparison, a 3% non-Poisson term was added in calculating the variance.) Thus, it was concluded that the low-temperature structure deviates only very slightly from orthorhombic symmetry, and orthorhombic space groups have been adopted throughout the subsequent analysis.

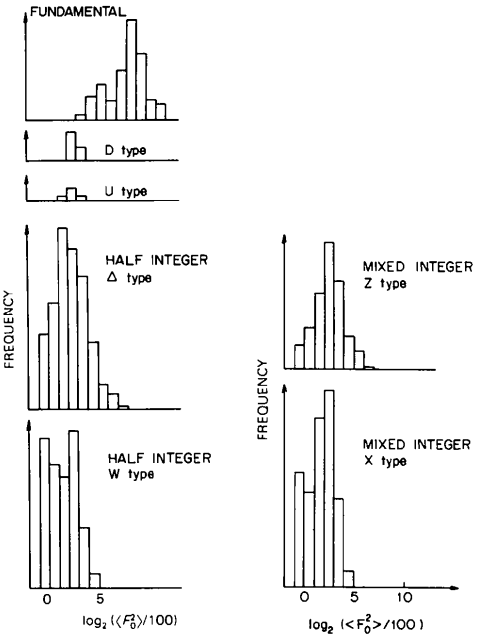

Fig. 2. Histogram distributions of $\log_2(\langle F_o^2 \rangle/100)$ for the various reflection classes.

The reflections were classified into fundamental, Δ, W, X and Z types as described above, and sorted on $\langle F_o^2 \rangle$ to obtain the histograms shown in Fig. 2. These distributions indicate that the W- and X-type superlattice reflections are generally weak in comparison to the Δ and Z type, and that the Δ type in turn includes somewhat stronger reflections than the Z type. This suggests that the atomic displacements generating the Δ-type half-integer reflections play a primary role in the lattice distortion below T_V, and that the displacements which cause the Z-type mixed-integer reflections are also important. The D- and U-type fundamental reflections are very weak and severely contaminated by multiple diffraction from the strong fundamental reflections, as will be seen below.

Refinement

Analysis of the low-temperature structure of magnetite is complicated by the presence of a high degree of pseudosymmetry. The low-temperature structure may be generated from the prototype cubic inverse spinel structure by means of small displacements. Although these displacements break most of the symmetry

elements possessed by the prototype, because the shifts are small the structure still maintains approximate higher symmetry.

The low-temperature structure retains the following pseudosymmetry elements:*

(i) face-centered cubic lattice translation in the base plane: $\{E|\mathbf{t}_{f.c.c.}\}$, where $\mathbf{t}_{f.c.c.} = \frac{1}{2}\mathbf{a}_M, \frac{1}{2}\mathbf{b}_M$;

(ii) mirror plane perpendicular to $\mathbf{a}_M$: $\{\sigma_a|\mathbf{t}_{f.c.c.}\}$; and

(iii) glide plane perpendicular to $\mathbf{c}_M$.

There are two choices of the glide plane that corresponds to a diamond glide in the prototype structure:

(iii-1) **a** glide: $\{\sigma_c|\frac{1}{2}\mathbf{a}_M + \frac{1}{2}\mathbf{c}_M\}$; or

(iii-2) **b** glide: $\{\sigma_c|\frac{1}{2}\mathbf{b}_M + \frac{3}{4}\mathbf{c}_M\}$.

These pseudosymmetry elements may be combined with the **c** glide to yield a variety of approximate space groups as indicated in Fig. 3. The pseudotranslation (i) causes the unit cell to be primitive with size $a/\sqrt{2} \times a/\sqrt{2} \times 2a$, the pseudomirror (ii) leads to orthorhombic space groups, and the pseudoglide (iii) to centrosymmetric groups. It is difficult to distinguish among space groups with the same cell size based upon systematic extinctions, due to the substantial contribution of simultaneous reflections at many reciprocal-lattice points.

The strategy adopted here in analyzing the low-temperature structure is to assign approximate space groups of relatively high symmetry, within which it may be possible to obtain a satisfactory explanation of the more intense superlattice reflections. The essential pattern of the displacements should be manifested in these approximate structures.

For Fe_3O_4, as mentioned in the experimental section above, the Laue symmetry is found to be very nearly *mmm* although the neutron diffraction measurements indicate that the low-temperature structure is actually monoclinic. Furthermore, because the *W*- and *X*-type superlattice reflections are found to be relatively weak these have been neglected, and analysis of the low-temperature structure restricted to the consideration of primitive orthorhombic space groups with a unit-cell size $a/\sqrt{2} \times a/\sqrt{2} \times 2a$, *i.e.* the centrosymmetric *Pmca* and *Pmcb*, and the polar $Pmc2_1$.

Details of the refinements are summarized in Table 2. The calculations were carried out with a general-purpose least-squares program in which derivatives of the structure factors with respect to the variable parameters are calculated numerically, in order to facilitate proper inclusion of the magnetic scattering. The total squared structure factor may be written as the sum of nuclear and magnetic parts:

$$|F_c|^2 = |F_n|^2 + q^2|F_m|^2 \qquad (7)$$

$$q^2 = 1 - (\boldsymbol{\eta}.\boldsymbol{\kappa})^2,$$

where $\boldsymbol{\kappa}$ is a unit scattering vector and $\boldsymbol{\eta}$ a unit vector along the spin direction or (0,0,1) in this case. The magnetic structure factor is

$$F_m = 0{\cdot}539 \sum_j S_j f_j\left(\frac{\sin\theta}{\lambda}\right) e^{-B^2\sin^2\theta/\lambda^2}\, e^{2\pi i(hx_j + ky_j + lz_j)}, \qquad (8)$$

where S_j and $f_j(\sin\theta/\lambda)$ are the spin in units of Bohr magnetons and the form factor of the jth Fe ion at (x_j,y_j,z_j) in the unit cell. $S_j = -2{\cdot}5$ for the *A*-site ions and

$$S_j = \tfrac{1}{2}(4{\cdot}5 \pm \Delta P_j) \qquad (9)$$

for *B*-site ions where ΔP_j is a change in the magnetic moment associated with the charge ordering. The magnetic form factor of the *B*-site ions was calculated as a mixture of Fe^{3+} and Fe^{2+} and the form factors given by Watson & Freeman (1961) were used in the calculation. Nuclear scattering lengths were taken to be $b_O = 5{\cdot}803$ and $b_{Fe} = 9{\cdot}51$ fm.

The least-squares procedure minimized the quantity

$$\sum_{hkl} w_{hkl}[\langle F_o^2(hkl)\rangle - k^2 y\,|F_c(hkl)|^2]^2, \qquad (10)$$

where weights were taken inversely proportional to the variance of each reflection estimated as follows

$$w_{hkl}^{-1} = \{\sigma_c^2[\langle F_o^2(hkl)\rangle] + [0{\cdot}02\langle F_o^2(hkl)\rangle]^2\} \qquad (11)$$

and values of F_o^2 were corrected for the effects of secondary extinction according to the formalism developed by Becker & Coppens (1974). The extinction was evaluated for $|F_n + qF_m|^2$ and $|F_n - qF_m|^2$ using an isotropic type I model with Lorentzian mosaic spread, and then averaged to give an overall correction term y that divides $\langle F_o^2\rangle$.

Due to the rather short wavelength $\lambda \simeq 0{\cdot}84$ Å (chosen in order to minimize effects of extinction) and

* The space-group operations are indicated by the Seitz space-group symbols $\{R|\mathbf{v}\}$ where R is a point-group operator and $\mathbf{v}$ is the translation vector associated with it.

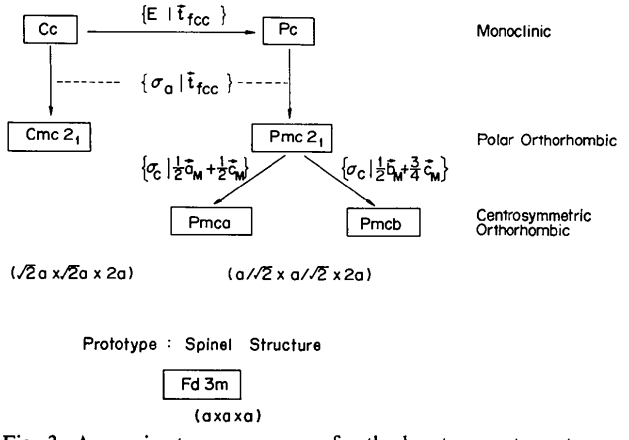

Fig. 3. Approximate space groups for the low-temperature structure, indicating the combinations of the pseudosymmetry elements with the **c** glide.

Table 2. *Details of refinements*

	Pmca				*Pmc*2_1			
		By reflection class				By reflection class		
	Overall	Fundamental	Δ type	Z type	Overall	Fundamental	Δ type	Z type
Number of observations (N_o)	573	169	271	133	576	169	271	136
Number of variables (N_v)	37				51			
$R = \sum \lvert\langle F_o^2\rangle - k^2 y \lvert F_c\rvert^2\rvert / \sum \langle F_o^2\rangle$	0·055	0·053	0·127	0·300	0·052	0·049	0·126	0·299
$R_w = [\sum w(\langle F_o^2\rangle - k^2 y \lvert F_c\rvert^2)^2 / \sum w\langle F_o^2\rangle^2]^{1/2}$	0·078	0·073	0·102	0·22	0·073	0·067	0·099	0·218
$S = [\sum w(\langle F_o^2\rangle / k^2 y - \lvert F_c\rvert^2)^2 / (N_o - N_v)]^{1/2}$	1·79				1·71			

large detector aperture employed in this experiment, it was anticipated that the probability of occurrence of simultaneous reflections would be rather high. In fact, the probability was sufficiently large that the intensity contributions from simultaneous diffraction appeared to be essentially uniformly distributed among reflections of a given type. This was demonstrated at various stages in the refinement process by plotting $\langle F_o^2\rangle$ *vs* $k^2 y \lvert F_c\rvert^2$. While the agreement is quite good for the main fundamental and stronger superlattice reflections, for both Δ and Z types $\langle F_o^2\rangle$ levels off to a threshold value as $\lvert F_c\rvert^2$ becomes very small. This level may be regarded as the average contribution from simultaneous diffraction of strong reflections of the same type. The observed squared structure factors of the D- and U-type weak fundamental reflections do not show any correlation with the calculated values and lie almost at the same level [*i.e.* about 400 in the arbitrary units of Fig. 2, corresponding to 74 fm^2 per primitive orthorhombic unit cell ($Z = 8$) on an absolute scale]. This clearly indicates the average contribution of simultaneous reflections from the strong fundamentals. The D- and U-type reflections were excluded from the subsequent analysis, while the threshold level was taken as a measure of the contribution of simultaneous reflections to the main group of fundamentals and subtracted from $\langle F_o^2\rangle$. For the Δ- and Z-type reflections, the threshold levels were estimated to be 37 and 74 fm^2, respectively. After the threshold values were subtracted, a few reflections with negative corrected $\langle F_o^2\rangle$ values were excluded, and the weights adjusted so that the e.s.d. of each reflection was at least as large as the threshold value.

Prior to collecting the three-dimensional diffraction data, selected reflections in high-symmetry scattering planes were measured carefully by suppressing the probability of simultaneous reflections through the use of long-wavelength incident neutrons, a tight collimator before the counter and in some cases by the use of the triple-axis geometry. The simultaneous reflections were carefully removed for lower-index reflections of the $h0l$ type by varying the incident neutron wavelength (Shirane *et al.*, 1975). Improved agreement was found between these 'high-resolution' observations and the calculated values obtained in the present structure analysis.

Trial structures for the initiation of refinements in the centrosymmetric space groups *Pmca* and *Pmcb* were generated from the cubic prototype by application of small atomic displacements derived from Yamada's (1975) model.

Space group Pmca

The first space group examined, *Pmca*, is a non-standard setting of *Pbcm* (No. 57). The asymmetric unit consists of two A-site Fe ions, four B-site Fe ions and six O^{2-} ions. These ions are assigned to positions with site symmetries indicated in Table 3: The origin of the unit cell is taken at the inversion center lying midway between two A sites. Altogether, this model requires that 23 positional parameters be determined. However, constraints were imposed in the initial stages of refinement, thereby reducing the number of variables, and these constraints removed in several steps during the refinement process.

An initial refinement varying eight positional parameters* led to convergence after several cycles, with a fairly good fit of the Δ-type superlattice reflections. The characteristic expansion and contraction in the structure assumed by Yamada was in general retained, although the displacements of the B-site Fe ions increased relative to the displacements of neighboring O^{2-} ions. However, the eight-parameter model did not fit the Z-type reflections at all. In the search for a trial structure incorporating features relevant to the Z-type reflections, the prominent intensities of the $22l$, $l = 2n + 1$ series provided a clue, and suggested a structure in which all O^{2-} ions at $z = \frac{1}{8}$ and all Fe ions at $z = \frac{3}{8}$ have positive z shifts, while all Fe ions at $z = \frac{1}{8}$ and O^{2-} ions at $z = \frac{3}{8}$ have negative z shifts. These displacements comprise a modulation of the structure with periodicity c, and are denoted as being of the Z type, while the displacements derived from Yamada's (1975) model have periodicity $2c$ and are of Δ type. Introduction of the Z-type displacements, followed by

* The variables were Δy for $A(1) = A(2)$, $B(2)$, $B(3) = B(4)$, O(3) = O(4), O(5), O(6) and Δz for $B(3) = -B(4)$ and O(3) = −O(4).

several cycles of least-squares refinement in which 11 positional parameters were varied,* gave a reasonable fit to the Z-type reflections. The characteristic pattern of displacements in the trial structure was again generally retained in the refined model.

At this point, the remaining constraints were removed and all 23 positional parameters were varied, together with isotropic thermal parameters for all atoms, which previously had been fixed at zero. Attempts were made to refine changes in magnetic moment for B-site Fe ions [ΔP_j in eq. (9)], but the resulting values had very high e.s.d.'s (of the order of 0·3) so that a reliable indication of the charge ordering could not be obtained. In the final cycles, ΔP_j values were fixed at zero. Scale and extinction-correction factors were varied throughout the refinement. The extinction was quite severe, with the correction term y reaching a minimum of 0·19 for reflection 040. An analysis of variance showed an increase in mean $|\langle F_o^2\rangle - k^2 y|F_c|^2|/\sigma(\langle F_o^2\rangle)$ for strong reflections, indicating that the extinction model was not entirely adequate, as might be expected. Final agreement factors are given in Table 2, while values of atomic coordinates and thermal parameters for the *Pmca* model are included in Table 3.† In the last cycle, the maximum shift in any parameter was of the order of $0{\cdot}1\sigma$, and a difference scattering-density synthesis computed at this stage was essentially featureless. (The largest peaks occurred near Fe ions, but these peaks were not significantly above the noise level.)

At various stages in the refinement process, attempts were made to test the uniqueness of the model. Some components of the displacements were intentionally reversed or set to zero and were refined again. The displacements kept unchanged always forced the model to recover the same final structure. Although these tests were by no means exhaustive, and certainly do not exclude the possibility of completely different types of structures, we have concluded that the refined structure is unique as long as the assumed Δ-type and Z-type modulations are basically correct.

Space group Pmcb

Refinements next were initiated in the alternative centrosymmetric space group *Pmcb*, a non-standard setting of *Pbam* (No. 55). The origin is again taken at a center of symmetry, thereby requiring a displacement of $-\frac{1}{4},\frac{1}{4},\frac{1}{8}$ relative to that in *Pmca*. Modification of Yamada's Δ-type displacements as required by space-group symmetry leads to a trial structure in *Pmcb* rather different from that in *Pmca*. In particular, due to the presence of the **b** glide at $z = \frac{1}{4}$, an alternating expansion and contraction of the B sites cannot occur at this level in the unit cell. Despite numerous attempts at refinement in *Pmcb*, it was not possible to obtain satisfactory agreement, particularly in the case of the Z-type reflections, for which the R value never went below 0·6.

Space group Pmc2$_1$

In the polar space group $Pmc2_1$ (No. 26), the assymmetric unit consists of four A-site and six B-site Fe ions, and 12 O^{2-} ions. The origin has been taken on the 2_1 axis at $-\frac{1}{8},-\frac{1}{8},0$ of the cubic unit cell, again in accord with standard conventions. The atoms were assigned to positions with site symmetries as indicated in Table 4. Starting from the *Pmca* model, an arbitrary shift was introduced in the z coordinate of one atom*

* In addition to the original eight parameters, the z coordinates of $B(4)$, O(5) and O(6) were refined at this stage.

† Lists of structure factors and interatomic distances and angles for *Pmca* and $Pmc2_1$ models have been deposited with the British Library Lending Division as Supplementary Publication No. SUP 36802 (15 pp.). Copies may be obtained through The Executive Secretary, International Union of Crystallography, 5 Abbey Square, Chester CH1 2HU, England.

* $B(2)$ was shifted, although any other atom would have served equally well.

Table 3. *Positional and thermal parameters from the Pmca refinement*

	Position above T_v*			Site	*Pmca* refinement			
	x	y	z	symmetry	x	y	z	B (Å^2)
$A(1)$	$\frac{1}{4}$	0	$\frac{1}{16}$	m	$\frac{1}{4}$	0·0049 (3)	0·0635 (1)	0·05 (4)
$A(2)$	$\frac{1}{4}$	$\frac{1}{2}$	$\frac{3}{16}$	m	$\frac{1}{4}$	0·5067 (2)	0·1887 (1)	0·05 (4)
$B(1)$	0	$\frac{1}{2}$	0	$\bar{1}$	0	$\frac{1}{2}$	0	0·13 (5)
$B(2)$	0	0	$\frac{1}{4}$	2	0	0·0099 (3)	$\frac{1}{4}$	0·14 (5)
$B(3)$	$\frac{1}{4}$	$\frac{1}{4}$	$\frac{3}{8}$	m	$\frac{1}{4}$	0·2643 (4)	0·3789 (1)	0·10 (3)
$B(4)$	$\frac{1}{4}$	$\frac{3}{4}$	$\frac{3}{8}$	m	$\frac{1}{4}$	0·7549 (5)	0·3746 (2)	0·01 (3)
O(1)	$\frac{1}{4}$	$\frac{1}{4}+\delta$	$-\delta'$	m	$\frac{1}{4}$	0·2630 (6)	−0·0027 (2)	0·16 (6)
O(2)	$\frac{1}{4}$	$\frac{3}{4}-\delta$	$-\delta'$	m	$\frac{1}{4}$	0·7477 (6)	−0·0009 (2)	0·13 (6)
O(3)	$\frac{1}{4}$	$\frac{1}{4}-\delta$	$\frac{1}{4}+\delta'$	m	$\frac{1}{4}$	0·2461 (7)	0·2540 (2)	0·27 (6)
O(4)	$\frac{1}{4}$	$\frac{3}{4}+\delta$	$\frac{1}{4}+\delta'$	m	$\frac{1}{4}$	0·7696 (6)	0·2527 (2)	0·20 (5)
O(5)	$-\delta$	0	$\frac{1}{8}+\delta'$	1	−0·0116 (6)	0·0089 (3)	0·1295 (2)	0·17 (5)
O(6)	$-\delta$	$\frac{1}{2}$	$\frac{1}{8}-\delta'$	1	−0·0067 (6)	0·5050 (3)	0·1244 (1)	0·11 (5)

* $\delta = 4\delta' = 0{\cdot}0096$.

Table 4. *Positional and thermal parameters from the Pmc2$_1$ refinement*

	Position above T_v*			Site	$Pmc2_1$ refinement			
	x	y	z	symmetry	x	y	z	B (Å^2)†
$A(1)$	0	0	$\frac{5}{16}$	m	0	0·0026 (14)	0·4370 (8)	0·05
$A(2)$	$\frac{1}{2}$	0	$\frac{1}{16}$	m	$\frac{1}{2}$	0·0065 (13)	0·0640 (7)	0·05
$A(3)$	$\frac{1}{2}$	$\frac{1}{2}$	$\frac{3}{16}$	m	$\frac{1}{2}$	0·5087 (12)	0·1891 (8)	0·08
$A(4)$	0	$\frac{1}{2}$	$\frac{7}{16}$	m	0	0·5044 (13)	0·3117 (7)	0·08
$B(1)$	$\frac{1}{4}$	$\frac{1}{2}$	0	1	0·2539 (14)	0·5027 (14)	−0·0002‡	0·13
$B(2)$	0	$\frac{1}{4}$	$\frac{1}{8}$	m	0	0·2597 (14)	0·1213 (7)	0·10
$B(3)$	0	$\frac{3}{4}$	$\frac{1}{8}$	m	0	0·7603 (14)	0·1263 (7)	0·01
$B(4)$	$\frac{1}{4}$	0	$\frac{1}{4}$	1	0·2433 (12)	0·0098 (5)	0·2476 (10)	0·14
$B(5)$	$\frac{1}{2}$	$\frac{1}{4}$	$\frac{3}{8}$	m	$\frac{1}{2}$	0·2680 (12)	0·3787 (7)	0·10
$B(6)$	$\frac{1}{2}$	$\frac{3}{4}$	$\frac{3}{8}$	m	$\frac{1}{2}$	0·7504 (15)	0·3753 (9)	0·01
O(1)	0	$\frac{1}{4}+\delta$	δ'	m	0	0·2484 (24)	0·0012 (9)	0·13
O(2)	$\frac{1}{2}$	$\frac{1}{4}+\delta$	$-\delta'$	m	$\frac{1}{2}$	0·2686 (23)	−0·0032 (9)	0·16
O(3)	0	$\frac{3}{4}-\delta$	δ'	m	0	0·7439 (22)	0·0020 (9)	0·16
O(4)	$\frac{1}{2}$	$\frac{3}{4}-\delta$	$-\delta'$	m	$\frac{1}{2}$	0·7440 (24)	−0·0006 (9)	0·13
O(5)	$\frac{1}{4}-\delta$	0	$\frac{1}{8}+\delta'$	1	0·2407 (18)	0·0085 (16)	0·1291 (12)	0·17
O(6)	$\frac{1}{4}-\delta$	$\frac{1}{2}$	$\frac{1}{8}-\delta'$	1	0·2449 (21)	0·5067 (16)	0·1239 (6)	0·11
O(7)	0	$\frac{1}{4}-\delta$	$\frac{1}{4}-\delta'$	m	0	0·2356 (20)	0·2464 (11)	0·27
O(8)	$\frac{1}{2}$	$\frac{1}{4}-\delta$	$\frac{1}{4}+\delta'$	m	$\frac{1}{2}$	0·2563 (18)	0·2555 (10)	0·27
O(9)	0	$\frac{3}{4}+\delta$	$\frac{1}{4}-\delta'$	m	0	0·7761 (24)	0·2492 (10)	0·20
O(10)	$\frac{1}{2}$	$\frac{3}{4}+\delta$	$\frac{1}{4}+\delta'$	m	$\frac{1}{2}$	0·7638 (24)	0·2549 (10)	0·20
O(11)	$\frac{1}{4}+\delta$	0	$\frac{3}{8}-\delta'$	1	0·2640 (21)	0·0096 (17)	0·3706 (10)	0·17
O(12)	$\frac{1}{4}+\delta$	$\frac{1}{2}$	$\frac{3}{8}+\delta'$	1	0·2575 (19)	0·5042 (15)	0·3755 (6)	0·11

* $\delta = 4\delta' = 0{\cdot}0096$.
† Isotropic thermal parameters were fixed at values from the *Pmca* refinement, Table 3.
‡ The z coordinate of $B(1)$ was fixed.

and refinements were carried out, first varying all the z parameters except that of $B(1)$ which was fixed in order to determine the origin, and then allowing all 49 positional parameters to vary.* Although the resulting e.s.d.'s are several times higher than for the *Pmca* case, the $Pmc2_1$ refinement converged fairly well and the overall R_w value decreased to 0·073 (see Table 2). The improvement in fit to the data over the *Pmca* model is modest; however, it is judged to be significant by Hamilton's (1965) criterion. In the last cycles, the shifts in all parameters were less than $1{\cdot}2\sigma$.† Final values of the atomic coordinates are given in Table 4, in which the coordinates have been adjusted so that the center of mass of the unit cell remains fixed in the polar direction.‡

Results and discussion

The displacements of ions from the positions in the prototype spinel structure are illustrated schematically in Fig. 4. The Fe–O distances‡ are indicated in Fig. 5 (*Pmca* model) and in Fig. 6 ($Pmc2_1$). The displacement pattern in both space groups is complex, and there is no significant variation in mean Fe–O distances for the octahedral B sites, such as might be expected to accompany charge ordering. In fact, mean Fe–O distances for both A and B sites are generally within one e.s.d. of the values from the prototype structure. Individual Fe–O distances calculated from the $Pmc2_1$ model show more variation than do those from *Pmca*; however, as was noted earlier, e.s.d.'s are also much larger for $Pmc2_1$, by about a factor of five. For the tetrahedral A sites, Fe–O distances from the *Pmca* model show an interesting trend: two distances, to the O^{2-} ions with larger z coordinates than the Fe ion, are about 0·03 Å longer than the distances to the two O^{2-} ions with smaller z coordinates. This trend is somewhat more difficult to discern in the $Pmc2_1$ model, but is still preserved in the case of $A(1)$ and $A(4)$. For both models, O–Fe–O angles around the A sites show only minor deviations from the tetrahedral value, 109·5°. However, for the B sites the deviations from the values in the cubic structure (87·7, 92·3 or 180°) are much larger, in several cases ranging up to 5° or more, reflecting the substantial displacements in coordinates for B-site Fe ions, particularly in the **b** direction.

According to the soft-phonon concept of displacive-type structural phase transitions, a low-temperature, distorted crystal structure is generated from a high-temperature, prototype structure by the condensation

* When the isotropic thermal parameters were allowed to vary, factors for a few atoms tended to become slightly negative, so in the last cycles all thermal parameters were fixed at their *Pmca* values.

† Certain shifts tended to oscillate with magnitudes in the neighborhood of one e.s.d., and it was not possible to reduce the shifts further.

‡ See deposition footnote.

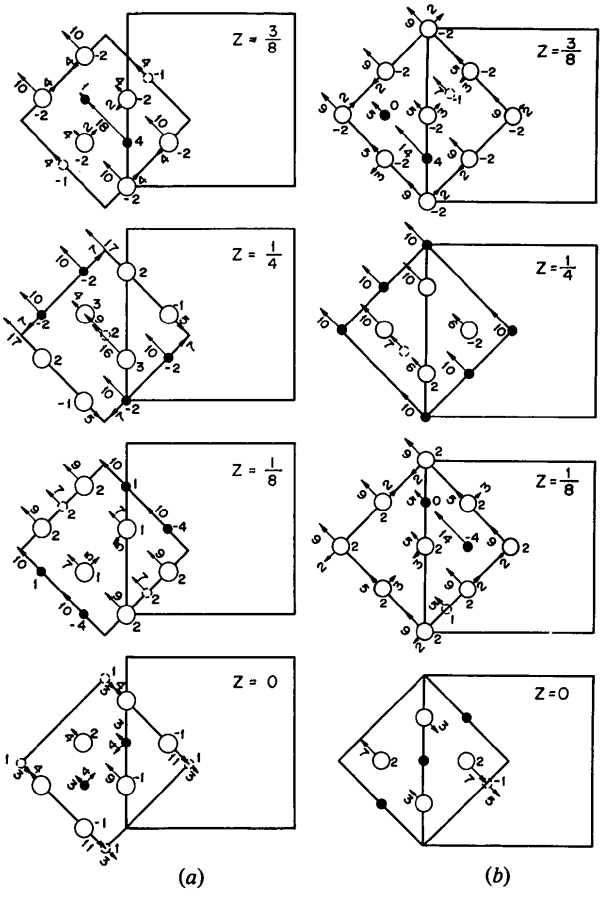

Fig. 4. Displacements from the cubic prototype structure below T_V: (*a*) refined model in space group $Pmc2_1$ (Table 4); (*b*) model in *Pmca* (Table 3). Displacements in x and y are shown by arrows, and z displacements are also indicated. All displacements are in fractional coordinates $\times 10^3$. O^{2-} ions are shown as open circles, *B*-site Fe ions as full circles, and *A*-site Fe ions as dashed circles. The *A*-site Fe ions lie $\frac{1}{16}$ in z below the levels shown. The z values refer to the doubled unit cell.

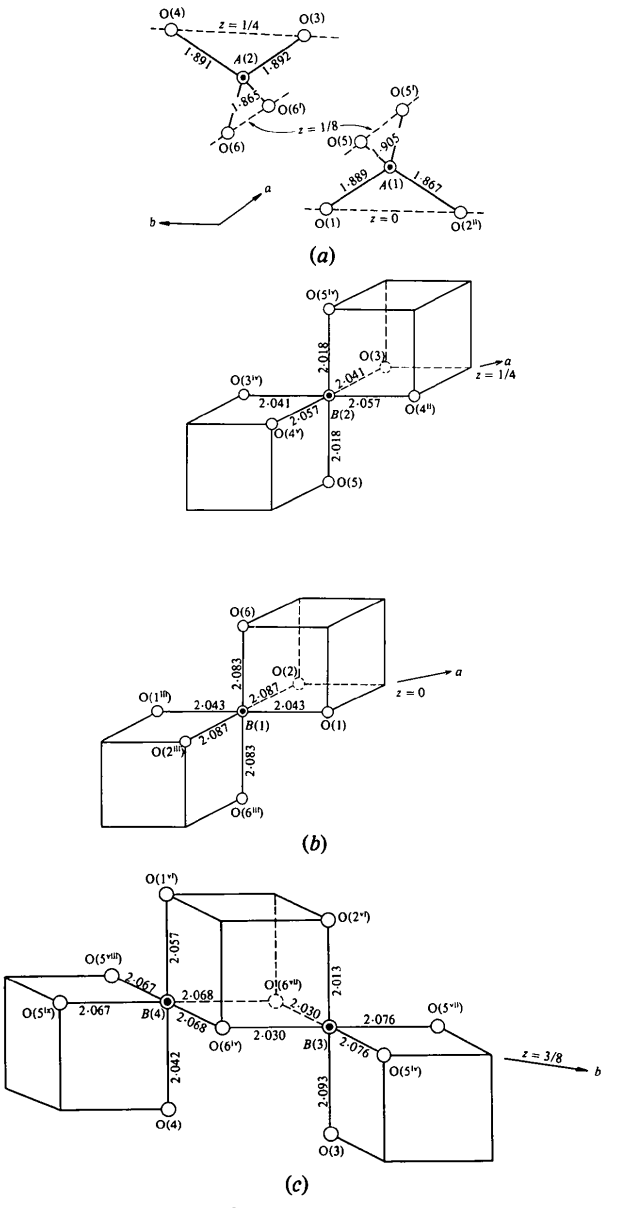

Fig. 5. Fe–O distances (Å) in the *Pmca* model. Positions related by symmetry to those given in Table 3 are denoted as follows: (i) $\frac{1}{2} - x, y, z$; (ii) $x, -1 + y, z$; (iii) $\bar{x}, 1 - y, \bar{z}$; (iv) $\bar{x}, y, \frac{1}{2} - z$; (v) $x, -1 + y, \frac{1}{2} - z$; (vi) $x, 1 - y, \frac{1}{2} + z$; (vii) $\frac{1}{2} + x, y, \frac{1}{2} - z$; (viii) $\frac{1}{2} + x, 1 + y, \frac{1}{2} - z$; (ix) $x, 1 + y, \frac{1}{2} - z$.

of a particular soft phonon that describes atomic displacements from the prototype to the distorted structure. Yamada's (1975) theory is an adaptation of this general concept to the Verwey transition in magnetite, based on condensation of a phonon belonging to the Δ_5 irreducible representation, as has been mentioned above. However, the complicated pattern of displacements in the low-temperature structure determined by the present neutron diffraction measurements is generated not by a single phonon condensation, but by concomitant condensation of a few phonons. A phonon with wavevector $\mathbf{q}_\Delta = (0,0,\frac{1}{2})$ contributes the dominant part of the atomic displacements, designated here as the Δ-type displacements. The remainder is contributed by another phonon with wavevector $\mathbf{q}_Z = (0,0,1)$, designated as the Z-type displacements. The Δ-type displacements give rise to the half-integer superlattice reflections, while the Z-type displacements are related to the odd–even mixed-integer superlattice reflections. The atomic displacements obtained for the $Pmc2_1$ model, being polar in nature, involve an additional phonon characterized by the zone center wavevector, $\mathbf{q}_\Gamma = (0,0,0)$. This latter component of the displacements is designated to be of Γ type.

The atomic displacements giving the low-temperature structure are a superposition of these three types of displacements defined above. The decomposition of the

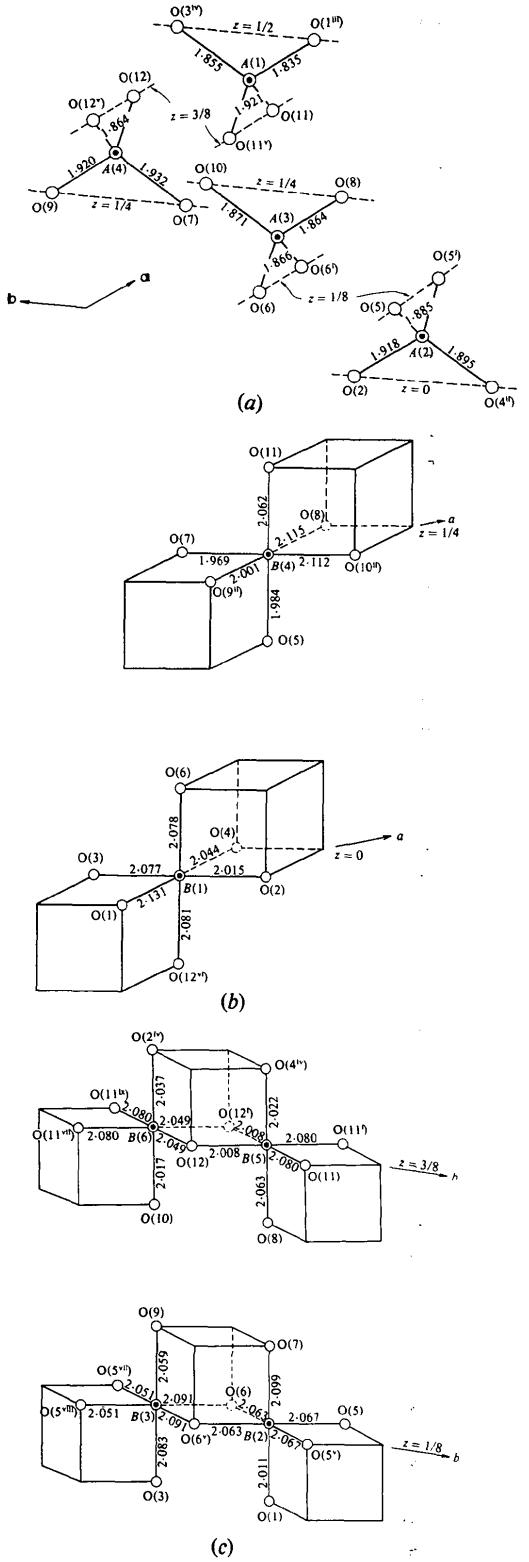

Fig. 6. Fe–O distances (Å) in the $Pmc2_1$ model. Positions related by symmetry to those given in Table 4 are denoted as follows: (i) $1-x, y, z$; (ii) $x, -1+y, z$; (iii) $\bar{x}, \bar{y}, \frac{1}{2}+z$; (iv) $x, 1-y, \frac{1}{2}+z$; (v) $\bar{x}, y, z$; (vi) $x, 1-y, -\frac{1}{2}+z$; (vii) $x, 1+y, z$; (viii) $\bar{x}, 1+y, z$; (ix) $1-x, 1+y, z$.

experimentally determined pattern can be carried out uniquely by taking the symmetry of each displacement into account. The result of the decomposition of the $Pmc2_1$ displacements is shown in Fig. 7.

The decomposition makes the general features of the displacement pattern easy to visualize. Although the original pattern is quite complex, each decomposed pattern possesses distinct features. The Δ-type displacements are similar in nature to the Yamada displacements. The principal components of the displacements lie along the **b** direction. The alternate contraction and expansion of the array of O^{2-} ions around the B-site Fe ions which form chains extending in the **b** direction is clearly visible at the level $z = \frac{3}{8}$. This pattern reflects the $\Delta_5^{(1)}$ mode which was proposed by Yamada (1975) and verified by neutron scattering measurements (Fujii *et al.*, 1974; Iizumi & Shirane, 1975). The wave nature of the Δ_5 displacement is clearly visible when the y displacements of the three kinds of ions are averaged separately at each level along the **c** direction. The result is shown in Fig. 8. The three displacement waves have a common phase and almost the same amplitude within the e.s.d.'s. The ions on the same level, therefore, displace almost in unison. The differences in displacements of individual ions cause the contraction and expansion mentioned above.

The Z-type displacements are characterized by the wavevector $\mathbf{q}_Z = (0,0,1)$ and are attributable to a zone-boundary phonon mode, which transforms according to the irreducible representation X_1. This is the set of displacements which has been proposed to exist by Iizumi & Shirane (1975) but has not previously been found. The existence of the Z-type displacements of X_1 symmetry together with the Δ-type displacements is very interesting, because it has been pointed out (Iizumi, 1979) that the concomitant condensation of the X_1 mode together with the Δ_5 mode is required for the intrinsically incommensurate Δ_5 mode to settle at the exact commensurate wavevector $\mathbf{q}_\Delta = (0,0,\frac{1}{2})$ when it condenses. The X_1-type lattice distortion furnishes the commensurability energy through the anharmonic coupling with the Δ_5-type lattice distortion. The diffuse-scattering measurements (Chiba, Suzuki & Chikazumi, 1975; Shapiro, Iizumi & Shirane, 1976) have already shown that there is a displacive fluctuation of the Z-type above T_V. Strong diffuse scattering has been observed at the X points (*e.g.* 722) together with the dominant diffuse scattering distributed within the disk or pancake regions around the strong Bragg points. The general proportionality of the intensity between the Z-type diffuse scattering above T_V and the superlattice reflections below T_V suggests that the displacive fluctuation at X points above T_V is of the Z (X_1) type indicated in Fig. 7.

Due to the relatively large e.s.d.'s in atomic positions in the $Pmc2_1$ model, the deduction of the Z- and Γ-type displacements yields components with magnitudes near

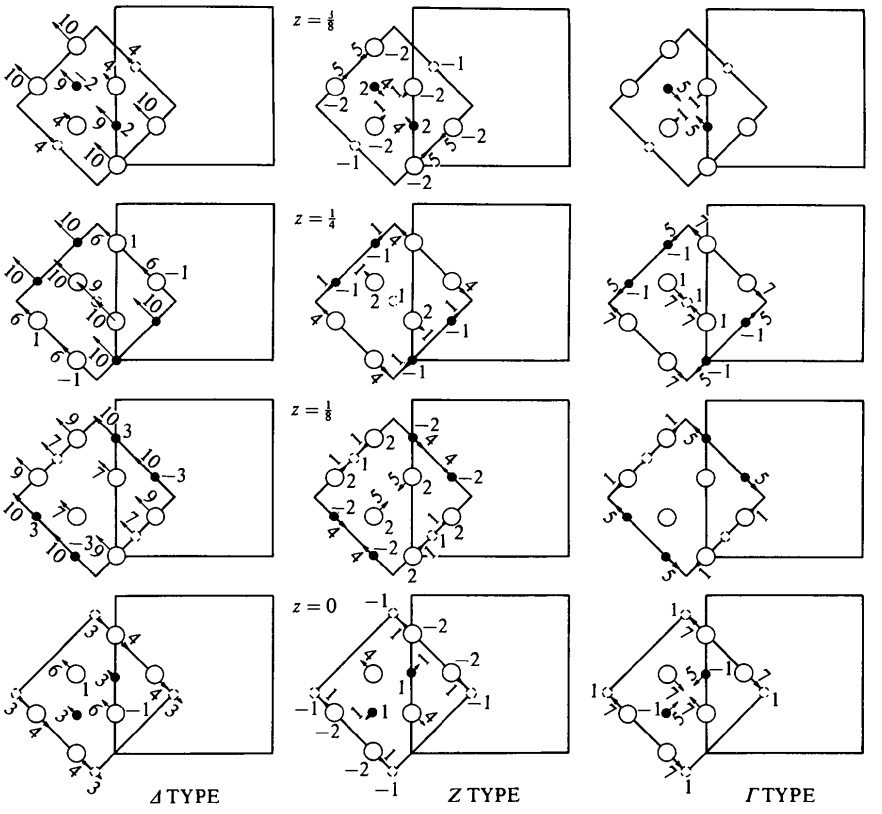

Fig. 7. Δ-, Z- and Γ-type components of displacements ($Pmc2_1$ model).

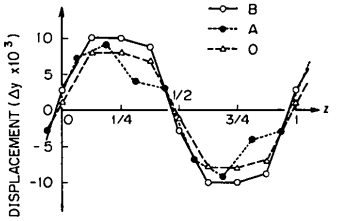

Fig. 8. $\Delta_5^{(1)}$ displacement wave, in which the average y displacements for each type of ion are plotted as a function of z ($Pmc2_1$ model).

the error limit. In spite of the large uncertainty, it is useful to examine the qualitative nature of the displacement patterns as shown in Fig. 7. The x and y components of the displacements are pairwise symmetric. A principal distinction is that the z components of the Γ-type displacements generate the spontaneous polarization while the Z type do not. Moreover, if we observe the collective distortion of cubes consisting of four B-site Fe ions and four O^{2-} ions [*e.g.* $B(1)$, $B(1^i)$, $B(5)$ and $B(6)$ and O(2), O(4), O(12) and O(12^i) with atomic labeling as defined in Fig. 6], we notice that there is an interesting distinction between the Γ- and Z-type displacements. The Γ type is characterized by the overall expansion or contraction of the cubes while the Z type is a sort of shear distortion. Part of the Γ-type displacements can be attributed to an optic phonon which transforms according to the Γ_{15} irreducible representation and condenses concurrently with the Δ_5 and X_1 modes at T_V. The coupling mechanism inducing the Γ_{15}-type distortion has not been clarified. Siratori *et al.* (1979) observed a large dielectric susceptibility with a long relaxation time at 77 K and suggested the existence of atomic displacements corresponding to an optic phonon. This may well be identified with the Γ-type displacements indicated here, although there is no evidence on the fluctuating properties of the displacements.

As has been mentioned in the description of the refinement procedure, the present analysis is based on approximate space groups in which a few pseudo-symmetry elements are assumed. Since these elements are eventually violated in the true structure, the results are approximate in the sense that the nonequivalent displacements in the true structure are replaced by an average displacement with respect to the pseudo-symmetry elements. The $Pmc2_1$ model is an approximation to the true space group Cc with respect to the orthorhombic symmetry and the f.c.c. translation in the base plane. Removing the f.c.c. translation we reach space group $Cmc2_1$ as indicated in Fig. 3. In this case

the asymmetric unit would be enlarged to include ten *B*-site Fe ions, and the superlattice reflections labeled earlier as *X* and *W* types would need to be included in the refinement. The resultant displacements would involve additional components: two of *X* type characterized by the wavevectors (1,0,0) and (0,1,0), and two of *W* type characterized by the wavevectors $(1,0,\frac{1}{2})$ and $(0,1,\frac{1}{2})$. However, the general weakness of the *X*- and *W*-type superlattice reflections (Fig. 3) implies that the magnitude of the *X*- and *W*-type displacements is small compared with the Δ and *Z* type, and that the former are unlikely to play a substantial role in the Verwey transition.

The orthorhombic symmetry is destroyed by removing the mirror plane perpendicular to the *a* axis. Pairs of equivalent ions related by the mirror planes in $Pmc2_1$ would then become independent and an asymmetric displacement pattern with respect to the mirror plane would be introduced. This asymmetry would cause discrepancies in intensity between reflections of the type $h_M k_M l_M$ and $h_M k_M \bar{l}_M$, *etc.* As mentioned earlier, discrepancies of this type are not significant, and the internal displacements must almost retain the mirror symmetry, even though the β angle differs slightly from 90°, reflecting the rhombohedral distortion of the original cubic unit cell. Elucidation of the pseudo-rhombohedral monoclinic distortions is beyond the scope of the present work.

As mentioned in the *Introduction*, the motivation of the present study was to provide the underlying crystal structure in order to allow the charge-ordering scheme to be determined unambiguously from a magnetic diffraction measurement. Although determination of the charge ordering is a separate and future task, some comments based upon the present analysis may be pertinent here. As was shown in eq. (1), the magnetic part of the diffraction intensity consists of two terms: the ΔP and $\bar{P}$ terms. However, in the present refinements only the $\bar{P}$ terms were found to contribute significantly to the calculated structure factors. When the ΔP terms were varied, very large e.s.d.'s were obtained. If alternate Fe^{2+} and Fe^{3+} charge ordering was assumed to occur along the chains of *B* sites extending in the **b** direction, the change in magnitude of ΔP was found to affect the fit only very marginally. Therefore, ΔP was set to zero in the final refinement. Intensities of some selected reflections, such as $2, 0, l + \frac{1}{2}$, which are most sensitive to the ΔP term for the assumed charge ordering, were calculated for the refined structure and compared with carefully measured intensities (Shirane *et al.*, 1975). These calculations indicated that the magnitude of ΔP should be $0{\cdot}2\ \mu_B$ at the very most.

The magnetic portion of the diffraction intensities of magnetite below T_V has been studied independently by the polarized neutron method (Shirane, Iizumi, Schweitzer & Chikazumi, 1976). The measured flipping ratios are in good agreement with the calculated values based on the low-temperature structure obtained in the present analysis. Since the polarized-beam measurements were limited to relatively high-index reflections, the magnetic part is predominantly contributed by the $\bar{P}$ term in eq. (1), and the agreement lends strong support to the structure determined by the present analysis. Now that reliable $\bar{P}$ terms have been obtained, proposed charge-ordering models can be strictly proved or disproved by a careful measurement of selected magnetic reflections pertinent to the models.

Quite recently Mizoguchi (1978*a*) carried out NMR measurements which indicated that the Fe^{3+} ions in the *B* sites are distributed among five nonequivalent sites, one of which is on the *B*-site chains along the *a* axis and four are on the chains along the *b* axis. To interpret these results, Mizoguchi proposed a unique charge-ordering scheme which consists basically of alternate Fe^{2+} pairs and Fe^{3+} pairs on the *B*-site chains along the *a* axis and a sequence of either three consecutive Fe^{2+} and one Fe^{3+}, or one Fe^{2+} and three consecutive Fe^{3+} on the chains along the *b* axis (Mizoguchi, 1978*b*). He determined the arrangement of the chains on the planes perpendicular to the *c* axis and the possible modes of stacking in the **c** direction. The resultant structure requires a primitive cell with the size of $\sqrt{2}a \times \sqrt{2}a \times 2a$ with no *C* centering. Mizoguchi's assertion that his charge-ordering scheme is consistent with the diffraction measurements with respect to the periodicity of the lattice is his misunderstanding, and his conclusion is clearly contradictory to our results in this respect. No actual intensities have been detected for superlattice reflections of the type $h + \frac{1}{2}, k, l$ or $h, k + \frac{1}{2}, l$ which are required to establish the doubling of the unit cell along the [100] and [010] directions of the cubic lattice. In a new scheme, proposed quite recently as an extension of the Mizoguchi model, Iida (1980) tried to avoid the conflict by introducing microscopic antiphase domains in the structure. The coherent sizes of the domains are random and too small for the internal structures to give rise to sharp superlattice reflections. Mizoguchi (1978*b*) has already employed a similar idea of microdomains in order to explain why the magnetic diffraction attributable to the proposed charge ordering is not observable. Nevertheless, these interpretations are questionable, because it is quite unlikely for the low-temperature structure to assume such a complicated artifact. The superlattice reflections originating from the atomic displacements are clearly observable and hence free from the microdomain, while the diffraction from the charge ordering closely coupled with the atomic displacements is not observable at all because of the microdomain. Since Mizoguchi's charge ordering is a unique conclusion once his assumptions are accepted, some of the assumptions, especially that the ion arrangement on the six nearest-neighbor *B* sites determines all aspects of the hyperfine field, should be open to question. Mizoguchi has pointed out that

without this assumption different types of charge ordering are possible.

In conclusion, the present analysis has established the essential features of the atomic displacements emerging below T_V. In particular, the constituent phonons composing the displacements are disclosed. The resultant structure gives a reliable estimate of the magnetic scattering component originating from the atomic displacements. This may afford a sound basis for determination of the charge-ordering scheme below T_V in the future.

This work was carried out while one of the authors (MI) was a visiting scientist at Brookhaven National Laboratory. He would like to express his gratitude to many colleagues in the Departments of Physics and Chemistry for their hospitality during this period. We would like to thank M. Mizoguchi for illuminating discussions and K. Chiba for helpful criticisms on the manuscript.

References

BECKER, P. J. & COPPENS, P. (1974). *Acta Cryst.* A**30**, 129–153.

BUSING, W. R. & LEVY, H. A. (1957). *Acta Cryst.* **10**, 180–182.

CHIBA, K., SUZUKI, K. & CHIKAZUMI, S. (1975). *J. Phys. Soc. Jpn*, **39**, 839–840.

CHIZAZUMI, S. (1976). *AIP Conf. Proc.* **29**, 382–387.

CHIKAZUMI, S., CHIBA, K., SUZUKI, K. & YAMADA, T. (1971). *Proceedings of the International Ferrite Conference*, Japan, p. 595. Tokyo Univ. Press.

DIMMLER, D. G., GREENLAW, N., KELLEY, M. A., POTTER, D. W., RANKOWITZ, S. & STUBBLEFIELD, F. W. (1976). *IEEE Trans. Nucl. Sci.* **23**, 385–405.

FUJII, Y., SHIRANE, G. & YAMADA, Y. (1974). *Phys. Rev. B*, **11**, 2036–2041.

HAMILTON, W. C. (1958). *Phys. Rev.* **110**, 1050–1057.

HAMILTON, W. C. (1965). *Acta Cryst.* **18**, 502–510.

IIDA, S. (1980). *Philos. Mag.* B**24**, 349–376.

IIDA, S., YAMAMOTO, M. & UMEMURA, S. (1973). *AIP Conf. Proc.* **18**, 913–917.

IIZUMI, M. (1979). *AIP Conf. Proc.* **53**, 184–186.

IIZUMI, M. & SHIRANE, G. (1975). *Solid State Commun.* **17**, 433–435.

International Tables for X-ray Crystallography (1968). Vol. III, 2nd ed., p. 197. Birmingham: Kynoch Press.

MCMULLAN, R. K. AND IN PART ANDREWS, L. C., KOETZLE, T. F., REIDINGER, F., THOMAS, R. & WILLIAMS, G. J. B. (1976). *NEXDAS*. Neutron and X-ray data acquisition system. Unpublished work.

MIZOGUCHI, M. (1978*a*). *J. Phys. Soc. Jpn*, **44**, 1501–1511.

MIZOGUCHI, M. (1978*b*). *J. Phys. Soc. Jpn*, **44**, 1512–1520.

RADO, G. T. & FERRARI, J. M. (1975). *Phys. Rev. B*, **12**, 5166–5174.

RADO, G. T. & FERRARI, J. M. (1977). *Phys. Rev. B*, **15**, 290–297.

SAMUELSEN, E. J., BLEEKER, E. J., DOBRZYNSKI, L. & RISTE, T. (1967). Kjeller Rep. KR-122. Institutt for Atomenergi, Kjeller, Norway.

SAMUELSEN, E. J., BLEEKER, E. J., DOBRZYNSKI, L. & RISTE, T. (1968). *J. Appl. Phys.* **39**, 1114–1115.

SHAPIRO, S. M., IIZUMI, M. & SHIRANE, G. (1976). *Phys. Rev. B*, **14**, 200–207.

SHIRANE, G., CHIKAZUMI, S., AKIMITSU, J., CHIBA, K., MATSUI, M. & FUJII, Y. (1975). *J. Phys. Soc. Jpn*, **39**, 949–957.

SHIRANE, G., IIZUMI, M., SCHWEITZER, J. & CHIKAZUMI, S. (1976). Unpublished work.

SIRATORI, K., KITA, E., KAJI, G., TASAKI, A., KIMURA, S., SHINDO, I. & KOHN, K. (1979). *J. Phys. Soc. Jpn*, **47**, 1779–1787

TOOMBS, N. C. & ROOKSBY, H. P. (1951). *Acta Cryst.* **4**, 474–475.

VERWEY, E. J., HAAYMAN, P. W. & ROMEIJAN, F. C. (1947). *J. Chem. Phys.* **15**, 181–187.

VIELAND, L. J. (1975). *Acta Cryst.* A**31**, 753–755.

WATSON, R. E. & FREEMAN, A. J. (1961). *Acta Cryst.* **14**, 27–37.

YAMADA, T., SUZUKI, K. & CHIKAZUMI, S. (1968). *Appl. Phys. Lett.* **13**, 172–174.

YAMADA, Y. (1975). *AIP Conf. Proc.* **24**, 79–85.

YOSHIDA, J. & IIDA, S. (1976). *J. Phys. Soc. Jpn*, **42**, 230–237.